Path-Length-Resolved Diffusive Particle Dynamics in Spectral-Domain Optical Coherence Tomography

J. Kalkman[1,*]

[1]*Biomedical Engineering & Physics, Academic Medical Center, University of Amsterdam, P.O. Box 22700, 1100 DE Amsterdam, The Netherlands*

R. Sprik[2]

[2]*Van der Waals-Zeeman Instituut, Universiteit van Amsterdam, Valckenierstraat 65, 1018 XE Amsterdam, The Netherlands*

T. G. van Leeuwen[1,3]

[3]*Biomedical Photonic Imaging, MIRA Institute for Biomedical Technology & Technical Medicine, University of Twente, P.O. Box 217, 7500 AE Enschede, The Netherlands*

(Received 1 March 2010; revised manuscript received 22 July 2010; published 5 November 2010)

We describe a new method to measure the decorrelation rate of the optical coherence tomography (OCT) magnitude simultaneously in space and time. We measure the decorrelation rate of the OCT magnitude in a Fourier-domain OCT system for a large range of translational diffusion coefficients by varying the sphere diameter. The described method uses the sensitivity advantage of Fourier-domain OCT over time-domain OCT to increase the particle diffusion imaging speed by a factor of 200. By coherent gating, we reduce the contribution of multiple scattering to the detected signal, allowing a quantitative study of diffusive particle dynamics in high concentration samples. We demonstrate that this technique is well suited to image diffusive particle dynamics in samples with a complex geometry as we measure the morphology and diffusive particle dynamics simultaneously with both high spatial and high temporal resolution.

DOI: 10.1103/PhysRevLett.105.198302 PACS numbers: 47.57.eb, 83.85.Ei

The dynamics of particles, such as colloids, polymers, cells, and proteins, is studied in a great variety of fields ranging from rheology [1], microfluidics (lab on a chip) [2], and soft condensed matter [3] to biology [4] and medicine [5]. Fundamental physical, chemical, and biological processes such as turbulence, aggregation, crystallization, protein folding, chemical reactions, flow, and diffusion are studied in bulk media, near interfaces, or in porous media. Commonly used optical techniques to study particle dynamics are dynamic light scattering (DLS) [6] and low coherence interferometry (LCI). DLS and LCI provide excellent temporal resolution; however, both DLS and LCI yield only limited spatial information. In DLS, spatial information can be obtained only by moving a loosely focused optical beam over a bulk sample. In LCI, the reference mirror is kept stationary [7,8] or is moved over a small distance [9]. Therefore it provides highly localized information but only over a very limited spatial range. In addition, both DLS and LCI do not provide simultaneous spatial and temporal information of the particle dynamics.

Optical coherence tomography (OCT) is an optical imaging technique that is gaining widespread use in the clinical world for obtaining micrometer-resolution images of biological tissues up to a few millimeters deep [10]. OCT is based on low coherence interferometry, whereby the path length of the detected photons is measured and used to determine the geometrical location of the single backscattering event in the sample. Like LCI, in time-domain OCT the reference mirror is moved; however, instead of over a few microns, it is moved over a distance of a few millimeters. In this way the scattering amplitude is measured sequentially for all path lengths over the full imaging range, providing a high-resolution line scan of the sample. The potential (clinical) applicability of OCT was boosted by the invention of Fourier-domain OCT [11]. In Fourier-domain OCT the optical spectrum is measured either by sweeping the input source wavelength (swept-source OCT) or by measuring the output spectrum with a spectrometer and a camera (spectral-domain OCT). Fourier-domain OCT has a sensitivity advantage compared to time-domain OCT because of a shot noise reduction in the optical detection [12]. The use of Fourier-domain OCT resulted in an OCT design with fewer mechanical parts and a higher optical sensitivity. More importantly, Fourier-domain OCT made it possible to simultaneously measure morphology and dynamical properties from the complex-valued OCT signal. In OCT, the magnitude of the OCT signal in space is used to image the backscattered amplitude, which can be used to measure layer thicknesses, tissue birefringence [13], and tissue attenuation coefficients [14]. The phase of the OCT signal in space is used to determine the group refractive index (refractometry) [15]. The phase of the OCT signal in time is used to determine the Doppler flow [16,17]. In this work, we finalize the OCT acquisition diagram [magnitude (phase) versus time (space)] by

measuring the OCT magnitude in time and determine the translational diffusion coefficient from it.

Using a spectral-domain OCT setup, we measure in a sample consisting of particles in solution the power spectrum of the temporal fluctuations of the OCT magnitude simultaneously for all depths. In this way we measure sample morphology and diffusive particle dynamics at high speed and high spatial resolution simultaneously. In addition, we gain a sensitivity advantage for measuring path-length resolved particle dynamics similar to the case when time-domain OCT imaging systems were replaced by Fourier-domain OCT systems. With these advantages the study of fundamental particle dynamics processes can be improved and measured in systems with a complex geometry.

In DLS, light from a long coherence length light source impinges on a homogeneous sample consisting of a low concentration solution of particles. The scattered light falls on a photodetector, and from the decorrelation rate of the intensity fluctuations, rotational and translational diffusion coefficients can be determined. For a heterodyne detection scheme, the intensity of single scattered light for translationally diffusing particles decorrelates at a rate of Dq^2; for a homodyne detection scheme, it decorrelates at a rate of $2Dq^2$ [18]. Here the diffusion coefficient D is given by the Stokes-Einstein equation $D = k_B T/6\pi\eta r$ with k_B Boltzmann's constant, T absolute temperature, η viscosity, and r the hydrodynamic particle radius. The scattering vector q is given by $q = |\vec{q}| = 2|\vec{k}|\sin(\theta/2) = 4\pi n \sin(\theta/2)/\lambda$, with n the refractive index of the medium, λ the wavelength in vacuum, and θ the scattering angle.

In its most basic form, Fourier-domain OCT is based on a heterodyne detection scheme using a Michelson interferometer with a broadband light source, a sample arm, a stationary reference arm, and a detector in the detection arm that can distinguish the different source wavelengths. In spectral-domain OCT, the mixing of the reference and the sample arm field is measured with a spectrometer that measures an optical spectrum in time with N light intensities $I_n(t)$, with n the pixel number (corresponding to a particular wavelength). We assume every intensity $I_n(t)$ to have infinite temporal coherence and to be independent. The depth-resolved scattering amplitude $a_{\mathrm{OCT}}(z, t)$ is determined by an inverse Fourier transformation of the measured optical spectrum [11]

$$a_{\mathrm{OCT}}(z, t) = \sum_{n=0}^{N-1} I_n(t) e^{2\pi i z(n/N)}. \quad (1)$$

The variation of the complex-valued OCT amplitude in space and time represents all the information available in OCT. In the spectral domain, Eq. (1) shows that the real and imaginary parts of the OCT amplitude both are proportional to a sum of detected heterodyne intensities, with every intensity decorrelating at a rate Dq_n^2. In OCT the spread in q_n is small, so we approximate the scattering vectors q_n with q_c at the center wavelength λ_c of the broadband OCT light source spectrum. Also, since the scattering amplitude $a_{\mathrm{OCT}}(z, t)$ in Eq. (1) is proportional to the particle density at position z, it is expected that the real and imaginary parts of $a_{\mathrm{OCT}}(z, t)$ for a sample with diffusive particles decorrelate at a rate $D(z)q_c^2$ since the density fluctuations cause the decorrelation of the heterodyne intensity [18]. We have shown that the real and imaginary parts of $a_{\mathrm{OCT}}(z, t)$ decorrelate at a rate of Dq_c^2 [19]; however, in OCT imaging generally the OCT magnitude $|a_{\mathrm{OCT}}(z, t)|$ is taken as the backscattered signal.

$$|a_{\mathrm{OCT}}(z, t)| = \sqrt{a_{\mathrm{OCT}}(z, t) a^*_{\mathrm{OCT}}(z, t)} = \sqrt{\sum_{k,l=0}^{N-1} I_k(t) e^{2\pi i z(k/N)} I_l(t) e^{-2\pi i z(l/N)}}. \quad (2)$$

The OCT magnitude in Eq. (2) contains products of intensities I_k and I_l on different pixels k and l on the camera. Since both intensities are formed in a heterodyne light scattering geometry, they both decorrelate with a rate Dq_c^2. It is therefore expected that the product of the two intensities decorrelates at a rate $2Dq_c^2$. We measure the power spectral density of the OCT magnitude, which is the Fourier transform of the correlation function of $|a_{\mathrm{OCT}}(z, t)|$, i.e., a Lorentzian with half linewidth $2Dq_c^2$ [19].

In our experiments we use a home-built spectral-domain OCT setup operating at $\lambda_c = 1300$ nm. Most important for the current experiments are the number of pixels $N = 1024$ of the camera, the numerical aperture NA = 0.02 of the sample arm optics, the coherence length $l_c = 18\ \mu$m, and the measurement line rate $f_{\mathrm{line}} = 32$ kHz. A low NA reduces the variation in scattering vector $\vec{q}$, and the high line rate enables high speed acquisition of intensity fluctuations. More details about the setup can be found in Ref. [17]. As diffusive scatterers we use polystyrene microparticles (G. Kisker GbR) with diameters of 46 (10 wt. %), 100 (2.5 wt. %), 194 (2.5 wt. %), 384 (2.5 wt. %), and 625 nm (2.5 wt. %) diameter. For all five microsphere solutions we measure the OCT signal scattering coefficient $\tilde{\mu}_s$ in depth. For increasing sphere size we obtain $\tilde{\mu}_s = 0.05 \pm 0.02\,\mathrm{mm}^{-1}$, $\tilde{\mu}_s = 0.10 \pm 0.02\ \mathrm{mm}^{-1}$, $\tilde{\mu}_s = 0.78 \pm 0.04\ \mathrm{mm}^{-1}$, $\tilde{\mu}_s = 5.1 \pm 0.2\ \mathrm{mm}^{-1}$, and $\tilde{\mu}_s = 5.1 \pm 0.2\ \mathrm{mm}^{-1}$.

Figure 1(a) shows a typical OCT depth scan for a solution of 194 nm diameter polystyrene spheres in a cuvette. The OCT magnitude decreases as a single exponential with increasing optical path length. Figure 1(b) shows the power spectra for two cases. For the first case (top curve), we measure the power spectrum of the OCT magnitude at a single depth point for 4000 consecutive time points and repeat this measurement 10 times to determine the average and the standard deviation of the power spectrum. The Lorentzian half linewidth is $2Dq_c^2$. We choose the single depth point, indicated in Fig. 1(a), to avoid surface effects on the diffusion close to the interface and to avoid the detection of multiple scattering at larger depths; the latter can increase the width of the power

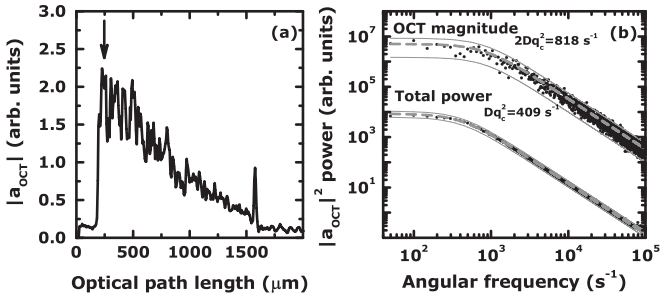

FIG. 1. (a) OCT magnitude A-line scan for a solution of 194 nm diameter spheres. The arrow indicates the location where the power spectrum in the spatial domain was taken and where the zero delay point was set for the total power measurement. (b) Power spectra for the OCT magnitude and for the total integrated power [single depth position and zero delay position indicated in (a) by the arrow]. Overlaid on the data are Lorentzian fits to the data (dashed gray line) with Dq_c^2 and $2Dq_c^2$ as half widths. The 3σ confidence intervals are indicated for both cases.

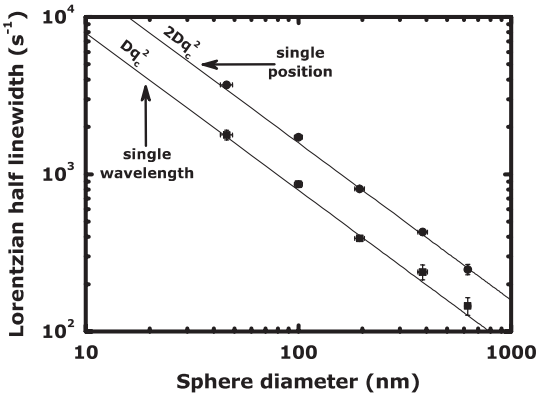

FIG. 2. Measured Lorentzian half linewidths for varying sphere diameter. The squares are for a measurement in the spectral domain (single wavelength); the circles are for a measurement in the spatial domain (single position). In the spectral domain the Lorentzian half linewidths are Dq_c^2 (see line). In the spatial domain the Lorentzian half linewidths are $2Dq_c^2$ (see line).

spectrum [20]. For the second case (bottom curve), we do a similar measurement, but we move the zero delay point to the same position as in the first case and calculate the power spectrum of the integrated total detected power (this situation is similar to the LCI experiment performed in Ref. [7]). Since OCT is performed in the heterodyne regime, with the reference power much larger than the sample power, the power spectrum in the second case should be a Lorentzian with a half width of Dq_c^2 (this measurement is equivalent to a heterodyne DLS experiment). Indeed we observe that the power spectrum of the integrated spectrum has a half width Dq_c^2. A confidence band of 3 times the standard deviation is indicated around the Lorentzians for both cases. The confidence band for the second case is a factor of 2.6 smaller than for the first case. However, in the spectral-domain OCT measurements we measure all 512 depths simultaneously in space and time. Consequently, we gain a factor of 200 in imaging speed compared to an LCI measurement with the same signal to noise ratio.

Figure 2 shows the measured Lorentzian half linewidths for various sphere diameters plotted on a double logarithmic scale, both for a measurement for a single wavelength (pixel) in the spectral domain and for a single depth in the spatial domain. A reciprocal relation between the sphere diameter and the Lorentzian half linewidth can be observed for both types of measurements, as expected from the Stokes-Einstein equation. The lines in Fig. 2 are calculated with Dq_c^2 and $2Dq_c^2$ as a function of the sphere diameter with $\eta = 0.9 \times 10^{-3}$ Pa s, $n = 1.33$, $T = 296$ K, $\lambda_c = 1300$ nm, $\theta = 180°$, where we assume single backscattering. The Lorentzian half linewidths for the largest sphere diameters measured in the spectral domain are slightly larger than predicted by theory. We attribute this to a small contribution of multiple scattering for these samples that have large scattering rates. Note that for a single wavelength all photon paths within the coherence length of a pixel are probed simultaneously, but that these effects are much smaller in the spatial domain where we only probe path lengths within the coherence length of the whole spectrum. Since multiple scattering effects increase with longer path lengths [17,20] we can, by choosing a spatial position close to the interface, reduce the optical path length through the scattering medium, thereby reducing multiple scattering effects. By coherence gating we can thus reduce multiple scattering effects and study higher concentration particle solutions, a significant advantage compared to DLS.

The range of sphere diameters where we can measure the decorrelation rate of the OCT magnitude $|a_{\mathrm{OCT}}(z, t)|$ and $2Dq_c^2$ is determined by the boundary conditions imposed by the experimental setup. First of all, the measured $|a_{\mathrm{OCT}}(z, t)|$ decorrelation rate should be lower than the Nyquist frequency of the sample frequency, in our case $2Dq_c^2 < f_{\mathrm{line}}/2$. Second, beat frequencies occurring on adjacent camera pixels can interfere due to spectral overlap between adjacent pixels. Because the imaging resolution of the OCT spectrometer is finite, some spectral overlap is present between wavelengths that are mapped onto adjacent pixels. In spectral-domain OCT this well known effect causes an additional roll-off of the system sensitivity with depth [21]. Our spectral-domain OCT system has a sensitivity roll-off, specified by the ratio ω of spectrometer resolution over pixel resolution, $\omega = 1.1$. Therefore, the power overlap between adjacent pixels is small (15% power overlap to an adjacent pixel), and, consequently, we do not expect a large influence of spectral overlap on the decorrelation rate. Similarly, because of the small spectral overlap between pixels, we can assume that their temporal behavior is independent [19], which supports our hypothesis on the factor of 2 in the decorrelation of $|a_{\mathrm{OCT}}(z, t)|$.

As an example of high speed spatially resolved particle dynamics imaging in a complex sample geometry, Fig. 3 shows OCT and diffusion imaging in practice for a sample

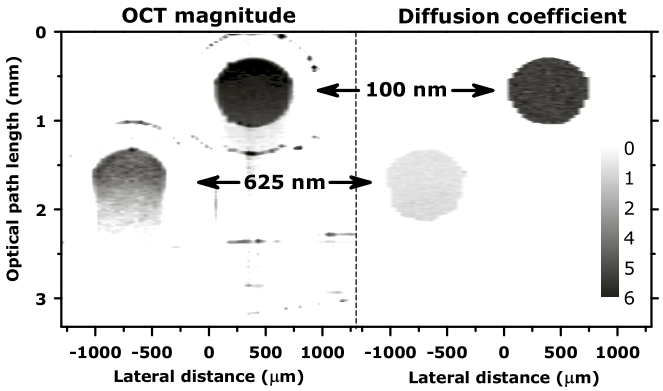

FIG. 3 (color online). OCT magnitude image (left) and diffusion coefficient image (right). The diffusion coefficient is determined only in the region of interest in the capillaries. The value of the diffusion coefficient, in units of $\mu m^2 s^{-1}$, is indicated in the legend in the diffusion image on the right.

consisting of two glass capillaries (550 μm inner diameter) submerged in water and filled with two microsphere solutions: 100 nm diameter (right) and 625 nm diameter (left). The whole OCT image (B scan) covers 64 A lines (512 depth points per A line). Every A line is measured at 4000 consecutive times points (127 ms per A line), and a power spectrum is calculated for every point in the spatial domain. This process is repeated 20 times and averaged. The total acquisition time for this B scan is 162 s (although more time was needed for processing). The OCT magnitude image (left) is used to determine a region of interest within the capillaries. For every point in the region of interest, the diffusion coefficient was determined by fitting the power spectrum with a Lorentzian using as fit parameters $2Dq_c^2$ for the half width, amplitude, and offset. The average diffusion coefficient in the two capillaries is 5.0 ± 0.3 (100 nm diameter) and 0.8 ± 0.2 $\mu m^2 s^{-1}$ (625 nm diameter). This is close to the theoretical prediction of 4.8 and 0.77 $\mu m^2 s^{-1}$ for these sphere diameters.

The high diffusion imaging speed that we show in Fig. 3 is significantly faster compared to that in Ref. [7]. However, a quantitative comparison is difficult, as there is a trade-off between imaging speed and the noise in the measured Lorentzian line shape; the latter is not defined in Ref. [7]. Yet, in our experiment the morphology and diffusion coefficient are measured simultaneously instead of sequentially, and we benefit from the spectral-domain over time-domain sensitivity advantage in OCT. In addition, our technique can be implemented in any Fourier-domain OCT system.

For quantitative diffusion imaging as shown in Fig. 3, multiple scattering, which occurs more at larger depths, is not included in the single scattering analysis. Also, the signal to noise ratio of the OCT signal should be sufficient to measure the power spectrum. Therefore, quantitative measurements deep into highly scattering solutions will be difficult. However, with recent advances in camera speed, removal of depth degeneracy, and shorter coherence length light sources, we expect the imaging performance of our method, in terms of signal to noise ratio, spatial, and temporal resolution, to be further improved in the future.

J. K. is supported by the IOP Photonic Devices program managed by the Technology Foundation STW and Agentschap NL.

*j.kalkman@amc.nl

[1] R. G. Larson, *The Structure and Rheology of Complex Fluids* (Oxford University, New York, 1999).
[2] G. M. Whitesides, Nature (London) **442**, 368 (2006).
[3] R. A. L. Jones, *Soft Condensed Matter* (Oxford University, New York, 2002).
[4] B. Jachimska, M. Wasilewska, and Z. Adamczyk, Langmuir **24**, 6866 (2008).
[5] J. Peetermans, I. Nishio, S. T. Ohnishi, and T. Tanaka, Proc. Natl. Acad. Sci. U.S.A. **83**, 352 (1986).
[6] W. Brown, *Dynamic Light Scattering: The Methods and Some Applications* (Clarendon, Oxford, 1993).
[7] D. A. Boas, K. K. Bizheva, and A. M. Siegel, Opt. Lett. **23**, 319 (1998).
[8] G. Popescu and A. Dogariu, Opt. Lett. **26**, 551 (2001).
[9] H. Xia, K. Ishii, T. Iwaii, H. Li, and B. Yang, Appl. Opt. **47**, 1257 (2008).
[10] D. Huang, E. A. Swanson, C. P. Lin, J. S. Schuman, W. G. Stinson, W. Chang, M. R. Hee, T. Flotte, K. Gregory, C. A. Puliafito, and J. G. Fujimoto, Science **254**, 1178 (1991).
[11] A. F. Fercher, C. K. Hitzenberger, G. Kamp, and S. Y. El-Zaiat, Opt. Commun. **117**, 43 (1995).
[12] T. Mitsui, Jpn. J. Appl. Phys. **38**, 6133 (1999).
[13] J. F. de Boer, T. E. Milner, M. J. C. van Gemert, and J. S. Nelson, Opt. Lett. **22**, 934 (1997).
[14] F. J. van der Meer, D. J. Faber, D. M. B. Sassoon, M. C. Aalders, G. Pasterkamp, and T. G. van Leeuwen, IEEE Trans. Med. Imaging **24**, 1369 (2005).
[15] A. V. Zvyagin, K. K. M. B. D. Silva, S. A. Alexandrov, T. R. Hillman, J. J. Armstrong, T. Tsuzuki, and D. D. Sampson, Opt. Express **11**, 3503 (2003).
[16] Z. Chen, T. E. Milner, S. Srinivas, X. Wang, A. Malekafzali, M. J. C. van Gemert, and J. S. Nelson, Opt. Lett. **22**, 1119 (1997).
[17] J. Kalkman, A. V. Bykov, D. J. Faber, and T. G. van Leeuwen, Opt. Express **18**, 3883 (2010).
[18] C. S. Johnson and D. A. Gabriel, *Laser Light Scattering* (Dover, New York, 1981).
[19] See supplementary material at http://link.aps.org/supplemental/10.1103/PhysRevLett.105.198302 for a document regarding the OCT signal decorrelation.
[20] K. K. Bizheva, A. M. Siegel, and D. A. Boas, Phys. Rev. E **58**, 7664 (1998).
[21] N. A. Nassif, B. Cense, B. H. Park, M. C. Pierce, S. H. Yun, B. E. Bouma, G. J. Tearney, T. C. Chen, and J. F. de Boer, Opt. Express **12**, 367 (2004).